CELL POKING

Determination of the Elastic Area Compressibility Modulus of the Erythrocyte Membrane

BILL DAILY AND ELLIOT L. ELSON
Department of Biological Chemistry, Division of Biology and Biomedical Sciences, Washington University School of Medicine, St. Louis, Missouri 63110

GEORGE IRENEUS ZAHALAK
Department of Mechanical Engineering, Washington University, St. Louis, Missouri 63130

ABSTRACT Cell poking, a new method for measuring mechanical properties of single cells was used to determine the elastic area compressibility modulus of osmotically swollen human erythrocytes. With this method we determined the force required to indent cells attached to a glass coverslip (Petersen, N. O., W. B. McConnaughey, and E. L. Elson, 1982, *Proc. Natl. Acad. Sci. USA*, 79:5327. Forces on the order of one millidyne and indentations on the order of one micron were detected. An analysis of these data in terms of a simplified mechanical model yielded the elastic area compressibility modulus. This analysis used a variational approach to minimize the isothermal elastic potential energy density function given by E. A. Evans and R. Skalak (Mechanics and Thermodynamics of Biomembranes, 1980, CRC Press, Boca Raton, FL). Measurements on swollen erythrocytes gave a range of values, depending in part on the osmotic conditions, of 17.9 ± 8.2 to 34.8 ± 12.0 mdyn/μm for the elastic area compressibility modulus at 25°C. Fractional area expansion >2.6 ± 0.8% produced rapid cell lysis. These values were not corrected for the reversible movement of water across the cell membrane in response to hydrostatic pressure gradients. Our results agree reasonably with those obtained by Evans et al. (Evans, E. A., R. Waugh, and L. Melnick, 1976, *Biophys. J.*, 16:585–595.) using micropipette aspiration under similar conditions.

INTRODUCTION

Many animal cell functions depend on the cell's ability to sustain and exert force. Deformability measurements on single cells can help to characterize how structural elements integrate cellular mechanical forces. A new technique called cell poking has been developed for making these measurements (1, 2). To apply this new approach to a cell system relatively amenable to a mechanical analysis and to compare these results with those already obtained by micropipette aspiration, we chose to investigate the mechanical properties of osmotically swollen human erythrocytes.

Conceptually the simplest mechanical experiment to perform, dilation of the mammalian red blood cell membrane by osmotic pressure has been investigated for over forty years (3). More recently, using micropipette aspiration, Evans et al. have carefully measured the elastic area compressibility modulus, K, of the red cell membrane. They report a value of 28.8 ± 5.0 mdyn/μm for K at 25°C under osmotic conditions similar to those we employ (4). In addition, they found that immediate lysis occurs for fractional area expansion of ~3 ± 0.7%. Subsequently they analyzed the effects of osmotic and hydrostatic pressure gradients created during aspiration (5). These gradients give rise to reversible movement of water across the cell membrane. Evans and Waugh report that the volume-corrected value of the area modulus is 45 mdyn/μm (5). In contrast, the membrane elastic shear modulus is much smaller, on the order of 10^{-3} mdyn/μm as suggested by data from both fluid shear flow (6) and micropipette aspiration experiments (7). From these experiments it is apparent that in the presence of large isotropic tensions, such as those experienced by osmotically swollen cells, the contribution of elastic shear forces to principal membrane force resultants is small.

This paper presents experimental data for the force required to indent swollen erythrocytes. From these data we derive the elastic area compressibility modulus of the red blood cell membrane based on a model developed by Evans and Skalak (8). We show that under reasonable simplifying assumptions the surfaces that minimize the elastic potential energy function of the cell membrane are also the surfaces that minimize surface area for constant interior volume. We also estimate the maximum fractional area expansion before rapid cell lysis.

Cell Poker

A description of a previous version of the cell poker has been published (2). The instrument used to make the measurements discussed below is illustrated in Fig. 1. A vertical glass stylus with tip (T) ~2 μm in diameter mounted on a horizontal glass fiber (W) ~3 cm in length is used to indent the cell (C). The horizontal fiber is attached to a linear piezoelectric motor (LPM). Optical sensors (MS and TS) monitor the vertical positions of the motor flag (MF) and the tip flag (TF). Cells on a glass coverslip are mounted in a thermostated chamber (TC), controlled to ±0.1°C. The experiment is observed through a microscope fitted with a X 32 Hoffmann modulation contrast objective (MO) and matching condenser (MC).

The horizontal fiber undergoes a vertical displacement in response to a varying voltage applied to the motor. As long as the tip is not in contact with the cell surface the output signals of the two sensors are identical. When contact occurs, the force exerted by the cell on the stylus reduces the stylus' displacement, bending the fiber slightly. From the displacement difference, X, between the tip and motor flags, we calculate the resistive force, F_w, using an independent calibration of the fiber bending stiffness, K_w, according to Hooke's Law, $F_w = K_w X$. Elastic moduli and coefficients of viscosity may be extracted with the aid of a mechanical analysis.

THEORY

Background

The equilibrium geometry of an unconstrained cell membrane subject to isothermal, reversible processes must be given by a minimum of a conservative potential energy functional. Evans et al. (8) have shown that, at constant chemical composition, the surface elastic potential is the sum of contributions from isotropic dilation or condensation of surface elements at constant element shape, deformation at constant element area, i.e., shear, local, and nonlocal curvature elastic effects. Due to the thinness of the membrane, the energy associated with bending is negligible except in deformations where the radii of membrane curvature approach the membrane thickness. In addition, Evans and Skalak (8) have demonstrated that the elastic modulus for area change, K, is at least several orders of magnitude greater than that for shear, μ. Furthermore, beam deflection experiments of Evans et al. (9) suggest that for loading conditions similar to those employed in cell poking the shear strain parameter, β, is small enough that $(2\,\mu\beta/K\alpha^2) \ll 1$ (8). This condition ensures that dilational energy contributions dominate those associated with shearing deformations throughout the membrane. Therefore, as a first approximation, shear and bending contributions to the surface free energy are neglected in the following simplified analysis; a more complete justification for this approach is provided in Appendix A.

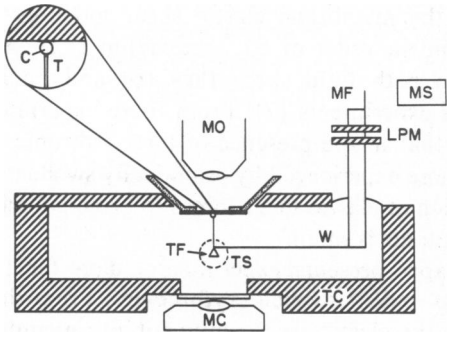

FIGURE 1 Schematic diagram of the cell-poker apparatus. *C*, cell; *T*, stylus tip; *W*, horizontal vycor glass fiber; *LPM*, linear peizoelectric motor; *MS* and *TS*, optical sensors; *MF*, motor flag; *TF*, tip flag; *TC*, thermostatted chamber; *MO*, modulation contrast objective; *MC*, matching condenser. (Reprinted with permission from Petersen, N. O., W. B. McConnaughey, and E. L. Elson, 1982, *Proc. Natl. Acad. Sci. USA.* 79:5327.

If the undeformed geometry of the cell is spherical and the interior volume is fixed, any deformation produces area dilation. Thus, for osmotically swollen erythrocytes constrained to approximate these conditions, we may express the elastic potential energy density in terms of a single deformation parameter, α ([8], Appendix A). In general, α is a local deformation parameter that measures the fractional change with respect to an undeformed "neutral" state in the area of material elements, element by element, over the surface. By neglecting shear contributions, we achieve a significant simplification in the analysis since in the absence of shear only an isotropic tension is supported by the membrane at equilibrium. In turn, it can be shown (10) that in-plane equilibrium of a membrane under isotropic surface tension requires that the tension be uniform; therefore, α is constant over the surface. Thus, α may be defined as the fractional change in area per molecule relative to the reference state.

Following Evans and Skalak (8) we expand the isothermal elastic potential energy density, $(\tilde{W})_T$, in a Taylor series. Assuming α is small, we have

$$(\tilde{W} - \tilde{W}_o)_T = \bar{T}_o\alpha + K\frac{\alpha^2}{2} + \dots \qquad (1)$$

where

$$\alpha = \frac{\tilde{A} - \tilde{A}_o}{\tilde{A}_o}$$

$$\bar{T}_o = \left(\frac{\partial \tilde{W}}{\partial \alpha}\right)_{T,\,\alpha=0}$$

$$K = \left(\frac{\partial^2 \tilde{W}}{\partial \alpha^2}\right)_{T,\,\alpha=0}$$

and $\tilde{A}$ is the surface area per molecule of the membrane in the deformed state. The subscript o refers to the reference state and the superscript ~ means per molecule. Then, we can identify the initial, undeformed state of a closed membrane system as the force-free state. Therefore, $\bar{T}_o$, the initial isotropic tension in the membrane for this reference state is set equal to zero. For a fixed number of molecules, N, the total change in elastic potential energy, U, is

$$(U - U_o)_T = KN\frac{(\tilde{A} - \tilde{A}_o)^2}{2\,\tilde{A}_o}. \qquad (2)$$

If $\tilde{A} \neq \tilde{A}_o$ this function is stationary only when the variation in surface area per molecule, $\tilde{A}$, vanishes. Therefore, the minimum energy geometry of the deformed surface is obtained by solving the variational problem that minimizes surface area at constant volume. Delaunay (11) showed that these solutions are contours of constant mean curvature, where the mean curvature is defined by $MK = 1/2(1/R_1 + 1/R_2)$, R_1 and R_2 being the principal radii of curvature at the point in question.

Appendix A presents a more elaborate mechanical analysis of cell poking using a variational approach similar to that outlined above. This

more elaborate analysis provides an explicit solution for the deformation field that allows us to establish an upper bound on the value of β characteristic of our measurements and to confirm that $(2\mu\beta/K\alpha^2) \ll 1$.

General Solution

Derivation of the General Solution. Assuming rotational symmetry about the z-axis, the appropriate functional may be written

$$A[z(r)] = 2\pi \int_{Rt}^{Rg} r\left[1 + \left(\frac{dz}{dr}\right)^2\right]^{1/2} dr + \lambda\left(V - 2\pi \int_{Rt}^{Rg} rz\, dr\right), \quad (3)$$

where the first term represents total surface area, the second enclosed volume, and λ is a Lagrange multiplier. The boundary conditions are specified in terms of Rt and Rg (Fig. 2), where Rt equals the radius of contact between the cell surface and the flat-ended cylindrical poker tip and Rg equals the radius of contact between the cell surface and the glass coverslip. Imposing boundary conditions like those shown in Fig. 2 *B* leads to double valued solutions. To facilitate calculations the functional is minimized in two parts, and the resulting solutions are matched at $z = 0$ by requiring continuity of the first derivative. Setting the functional derivative, $\delta A[z(r)]/\delta[z(r)]$, equal to zero yields the following Euler equation

$$\frac{d}{dr}\left[\frac{r\, dz/dr}{[1 + (dz/dr)^2]^{1/2}}\right] + \lambda r = 0.$$

Scaling out λ by the following change of variables $r = x/\lambda$, $z(r) = y(x)/\lambda$, and integrating this equation one time gives (see also Appendix A)

$$\pm\frac{dy}{dx} = \frac{x^2 + 2c_s}{[4x^2 - (x^2 + 2c_s)^2]^{1/2}}, \quad (4)$$

where c_s is the resulting scaled constant of integration. (Hereafter the subscript s denotes the scaled form of the noted variable.) Rearranging terms, y may be expressed as a linear combination of two indefinite elliptic integrals

$$\pm\int_{y(Rt_s)}^{y(x)} d\hat{y} = 2c_s \int_{Rt_s}^{x} \frac{d\hat{x}}{[(\gamma^2 - \hat{x}^2)(\hat{x}^2 - \omega^2)]^{1/2}} + \int_{Rt_s}^{x} \frac{\hat{x}^2\, d\hat{x}}{[(\gamma^2 - \hat{x}^2)(\hat{x}^2 - \omega^2)]^{1/2}}, \quad (5)$$

where $\omega = 1 - [1 - 2c_s]^{1/2}$, $\gamma = 1 + [1 - 2c_s]^{1/2}$, and Rt_s equals the scaled radius of contact between surface and probe tip with $\omega,\gamma: |\omega| < x < \gamma$. Hence, the general scaled solution, possessing two arbitrary constants, c_s and d_s, to be determined by imposing two boundary conditions, may be written using standard notation

$$\pm y = \omega F(\psi, k) + \gamma E(\psi, k) + d_s \quad (6)$$

where $F(\psi,k)$ equals the elliptic integral of the first kind, $E(\psi, k)$ equals the elliptic integral of the second kind, and $\psi = \sin^{-1}[(\gamma^2 - x^2)/(\gamma^2 - \omega^2)]^{1/2}$, $k = [(\gamma^2 - \omega^2)/(\gamma^2)]^{1/2}$.

Forms of the General Solution. Numerical evaluations of this equation exhibit three basic geometric forms: indented, spherical, and extended, depending on the boundary conditions imposed. Varying the constant, d_s, simply translates the membrane without change of shape, so we arbitrarily choose $d_s = 0$. Further, we locate the membrane with respect to the (r, z) coordinate system by requiring that the r-axis pierce the membrane at the point of vertical tangency so that $[dz/dr]_{z=0} = \pm\infty$. This sets the upper limit of x to γ. The constant, c_s, can be determined by a boundary condition at $y(Rt_s)$. For $(dy/dx)\big|_{Rt_s} < 0$, the contours are extended as shown in Fig. 2 *A*. For $Rt_s = 0$, the solution is a sphere. For $(dy/dx)\big|_{Rt_s} > 0$, the contours are indented as illustrated in Fig. 2 *B*. All solutions are solutions of constant mean curvature up to the boundary. The Lagrange multiplier, λ, is determined from the condition of constant volume

$$\lambda = \left[\frac{V_s}{V}\right]^{1/3}, \quad (7)$$

where V is the volume. The surfaces are scaled accordingly.

A Limiting Case. To confirm our numerical results, we seek an analytical form for the solution in the limiting case as c_s approaches 0.5. In this limit, ω approaches, γ, and the range of integration over x becomes a very short segment of the real axis about $x = 1$. In this range we let $\gamma = 1 + \epsilon$, $\omega = 1 - \epsilon$, and $x = 1 + \delta x$ where $-\epsilon < \delta x < \epsilon$. As $\gamma \to \omega$, $k \to 0$ and $E(\psi, k) \to F(\psi, k) \to \psi$ so that $y = (\omega + \gamma)\psi + \ldots = 2\psi + \ldots$. Furthermore,

$$\psi = \sin^{-1}\left[\frac{(1 + 2\epsilon + \ldots) - (1 + 2\delta x + \ldots)}{(1 + 2\epsilon + \ldots) - (1 - 2\epsilon + \ldots)}\right]^{1/2} = \sin^{-1}\left[\frac{1}{2}\left(1 - \frac{\delta x}{\epsilon}\right)\right]^{1/2} + \ldots.$$

So,

$$y = 2\sin^{-1}\left[\frac{1}{2}\left(1 - \frac{\delta x}{\epsilon}\right)\right]^{1/2} + \ldots. \quad (8)$$

Clearly, as δx varies from $-\epsilon$ to ϵ, y varies from $-\pi$ to π. Thus, as obtained numerically, this solution is a cylinder with a length-to-diameter ratio of π. This is an expression of the well-known observation that a cylinder with these dimensions represents a stability limit for the exten-

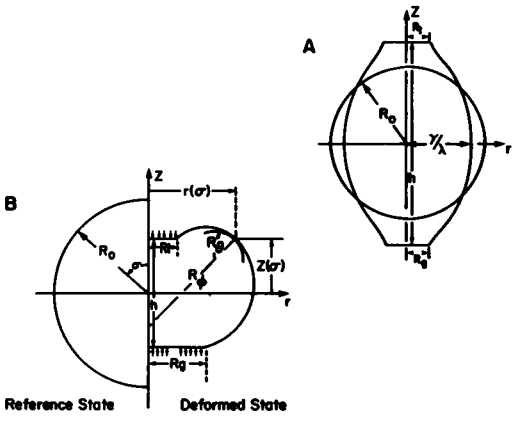

FIGURE 2 (*A*) Extended surface contour of constant mean curvature ($c_u = 0.19$, $Rt/R_o = Rg/R_o = 0.30$, $\gamma/\lambda R_o = 0.88$, $h/R_o = 2.72$, $\alpha = 0.025$, calculated assuming full cell inflation). (*B*) Indented surface contour of constant mean curvature ($c_u = 0.38$, $Rt/R_o = 0.30$, $Rg/R_o = 0.57$, $\gamma/\lambda R_o = 1.14$, $h/R_o = 1.15$, $\alpha = 0.068$, calculated assuming full cell inflation (r, z, ϕ), cylindrical coordinates with z-axis of symmetry; Rt, radius of contact between poker tip and cell surface; Rg, radius of contact between glass coverslip and cell; γ/λ, equatorial radius of the cell surface; h, height of the cell surface related to total displacement d by $d = 2R_o - h$; F, force exerted by the rigid supports on the cell.

sion of a fluid surface (12). In ideal liquid jets or cylindrical films, surface oscillations with length-to-cylinder diameter ratios $>\pi$ tend to grow in amplitude and eventually cause the cylinder to break up into droplets or bubbles (13).

Physical Interpretation of Parameters. We have investigated the possibility that the parameters λ and c_u ($c_u \equiv c_s/\lambda$), which arise naturally in this problem, have a simple physical interpretation. We have defined a scaling transformation $x = \lambda r$, $y = \lambda z$. Therefore, $(1/R_\theta + 1/R_\phi) = \lambda(1/R_\theta + 1/R_\phi)_s$. Furthermore, a straightforward calculation employing the following relations for the principal radii of curvature at a point on the membrane

$$\left(\frac{1}{R_\theta}\right)_s = \frac{d^2y/dx^2}{[1 + (dy/dx)^2]^{3/2}} \tag{9a}$$

$$\left(\frac{1}{R_\phi}\right)_s = \frac{dy/dx}{x[1 + (dy/dx)^2]^{1/2}} \tag{9b}$$

shows that $(1/R_\theta + 1/R_\phi)_s = 1$ for all values of c_s that yield real solutions. By convention, signs are chosen so that R_θ and R_ϕ are positive for the sphere. Thus, $\lambda = (1/R_\theta + 1/R_\phi)$. Moreover, using the equation of mechanical equilibrium for normal forces in the absence of shear (8)

$$\Delta P = \bar{T}\left(\frac{1}{R_\theta} + \frac{1}{R_\phi}\right), \tag{10}$$

where ΔP is the pressure difference across each element of surface area and $\bar{T}$ is the isotropic tension we also see that

$$\lambda = \frac{\Delta P}{\bar{T}}. \tag{11}$$

Thus, $\Delta P/\bar{T}$ is constant over the membrane since λ is taken to be constant.

A physical interpretation of the unscaled constant of integration, c_u, is also possible. Solving Eq. 4 for c_s and reintroducing the scaling factor λ gives

$$-c_u = \frac{\lambda r^2}{2} + \frac{r(dz/dr)}{[1 + (dz/dr)^2]^{1/2}}.$$

We may substitute the sum of Eqs. 9a and 9b in their unscaled forms for λ. This yields

$$c_u = \frac{r^2}{2}\left[\frac{d^2z/dr^2}{[1 + (dz/dr)^2]^{3/2}} - \frac{dz/dr}{r[1 + (dz/dr)^2]^{1/2}}\right]$$
$$= \frac{r^2}{2}\left(\frac{1}{R_\theta} - \frac{1}{R_\phi}\right).$$

For convenience, we choose to examine this relation for indented surfaces at the parabolic point $r = Rg$ where $1/R_\phi = 0$ and $1/R_\theta = \lambda$. Substituting Eq. 11 for λ gives

$$c_u = -\frac{\Delta P\, Rg^2}{2\bar{T}}. \tag{12}$$

As shown in the following section entitled Calculation of the Force Acting on the Poker Tip, the right-hand side of Eq. 12 is proportional to dA/dd, the differential change in surface area as the surface is indented by an amount dd. Thus, when multiplied by $-2\pi\bar{T}$, the unscaled constant of integration, c_u, has units of force and represents the load exerted by the cell on the poker tip. Numerical results suggest that this relation is also valid for extended surfaces as shown in Fig. 2 *A*. We note a sign change consistent with our interpretation of c_u as a force: c_u is greater than zero for extension, zero for the sphere, and less than zero for indentation. For a fixed value of the radius of contact between the cell surface and the probe tip, the limiting values of c_u for which real solutions exist correspond to stability limits of ideal surfaces that sustain no shear or bending forces (12).

We note the relation of the constants λ and c_u to the invariants of the surface curvature matrix. Two invariant parameters determine the values of the matrix elements for any orientation of the coordinates. These parameters may be defined as the mean and difference of the principal components of the matrix in its diagonal form. Thus, λ is twice the first invariant, and c_u is $r^2/2$ times the second invariant.

Application of the General Solution to Cell Poking

Imposition of Appropriate Boundary Conditions. The general solution for surfaces of minimum area and constant volume can be applied to cell poking. This requires that we impose the following boundary conditions on indented contours

$$\text{at } z(Rt) \text{ for } \begin{cases} Rz_{max} < Rt & dz/dr = 0 \quad (13a) \\ Rz_{max} \geq Rt & Rt = Rp \quad (13b) \end{cases}$$

$$\text{at } z(Rg) \quad \text{for all } Rz_{min} \quad dz/dr = 0 \quad (13c)$$

where $Rz_{max(min)}$ equals the value of r when $z(r)$ reaches its maximum (minimum) value and Rp equals the radius of the poker tip. Because the solution is double valued over this range of integration and because the boundary conditions are asymmetric with respect to the r-axis, we rewrite Eq. 4 evaluating first from $r = Rt$ to $r = \gamma/\lambda$ (where $z = 0$) and then from $r = \gamma/\lambda$ to $r = Rg$. Differentiability at γ/λ is assured by requiring that $dr/dz = \pm\infty$ at this point. Fig. 2 *B* shows a representative surface.

Calculation of the Force Acting on the Poker Tip. To determine K, the elastic area compressibility modulus, we derive a relation for the force, F, acting on the poker tip as a function of the displacement, d, of the tip ($d = 2R_o - h$ where h is defined as the distance between tip and coverslip, see Fig. 2 *B*). We can derive this relation either by taking the derivative of the surface potential energy function (8) with respect to the total displacement of the poker tip or by calculating the force directly from the required axial force balance. We have demonstrated that both approaches give identical results. In the first case

$$F = \left(\frac{\partial U}{\partial d}\right)_T = \frac{K\alpha}{A_o}\frac{\partial A}{\partial d}\int dA_o = K\alpha\frac{\partial A}{\partial d},$$

where α could be removed from under the integral sign since it is constant over the surface. As explained below, this gives $F = \bar{T}(\partial A/\partial d)$.

In the second case we use axial force balance equations as the basis for the derivation. This derivation requires a relation between the extensive force, F, acting on the poker tip, and the intensive force resultant, $\bar{T}$, acting on material elements. From the work of Evans and Skalak (8), we obtain the appropriate elastic constitutive equation, a relation between geometric variables and intensive force resultants

$$\bar{T} = \left[\frac{\partial \bar{W}}{\partial \alpha}\right]_T$$
$$= K\alpha + O(\alpha^2) + \ldots. \tag{14}$$

Since α is assumed to be small, only terms linear in α are retained. We can now calculate the total force acting on the poker tip from the required axial force balance. The force acting on the poker tip can be expressed as $F = 2\pi Rt\,\bar{T}\cos\phi + \Delta P(\pi Rt^2)$, where ϕ is the angle between the z-axis

and the tangent to the surface at the boundary of the contact region. However, at equilibrium the force acting in the positive z-direction on the poker tip must equal the force exerted in the negative z-direction by the cell on the glass coverslip. Since at this boundary $\cos \phi = 0$, F is given by $F = \Delta P\ (\pi R g^2)$. For convenience we calculate F from this relation. Substituting from Eqs. 10 and 14 gives

$$F = \pi R g^2\,(1/R_\theta + 1/R_\phi) \cdot K \cdot \alpha. \qquad (15)$$

Using Eq. 6 we obtain the deformed contours of minimum energy that yield the geometric parameters, α, Rg, R_θ, R_ϕ, and d. Using Eq. 15 we obtain F/K. Normalizing by the radius of the undeformed sphere, we have in dimensionless units

$$\frac{F}{K \cdot R_o} = \pi R g^2 \cdot \frac{(1/R_\theta + 1/R_\phi) \cdot \alpha}{R_o}. \qquad (16)$$

Then we can plot $F/K \cdot R_o$ or α as a function of d/R_o as shown in Fig. 3. We obtain a functional form for Eq. 16 by scaling to the dimensions of a swollen erythrocyte, $R_o = 3.4\ \mu$m (14), and interpolating the numerically generated points using a fourth order polynomial. We determine the elastic area compressibility modulus for the red blood cell membrane by fitting this function to data from cell poking experiments.

EXPERIMENTAL METHODS

Human erythrocytes were collected fresh each morning by fingerprick from healthy donors into a heparinized solution of 300 mOsm Dulbecco's phosphate-buffered saline, D-PBS (pH = 7.4). The cells were washed three times in D-PBS and resuspended at room temperature in the same buffer. Before poking, the cells were plated on glass coverslips covalently coated with polylysine (15). Polylysine provides a more secure attachment point for the erythrocyte, restricting its lateral motion during poking. After ~2 min, the coverslips were mounted with the cell side downward in the poking chamber containing D-PBS of known osmolality plus 2.5 mg/ml bovine serum albumin. The osmolalities of the D-PBS solutions used to swell the cells were measured with a vapor pressure osmometer. The cells rapidly swelled and measurements were made. All experiments were conducted at 25°C using a triangular waveform reference to drive the motor.

RESULTS

Fig. 4 shows an example of data obtained on a fully swollen erythrocyte. Fig. 4 *A* illustrates the time course of the vertical displacement of the stylus in the absence of contact between poker tip and cell surface. Fig. 4 *B* shows the result of cell contact. Fig. 4 *C* is a plot of the difference between the reference and cell data. This difference is proportional to the force exerted by the cell surface on the stylus tip as a function of time. Fig. 4 *D* shows the corresponding force vs. displacement data. Fig. 5 shows analogous data obtained on a less than fully swollen erythrocyte. In Figs. 4 and 5 the minimal hysteresis between the indentation and withdrawal phases of the poke suggests that the membrane mainly responds elastically. No significant alterations in this response were detected for rates of deformation that were fivefold faster or twofold slower than that shown in Fig. 4 (Table I). Furthermore, plastic effects were not routinely observed except in cells that lysed. A second or third poke on the same cell yielded a value for the fitted area compressibility modulus within 15% of the first. In a few cases, significant hysteresis was present, but we believe that this was primarily due to undetected lateral movement of the cell or to cell damage that may have resulted in substantial volume loss during a poke. The average rate of deformation (the rate of dilation or condensation of surface area) was on the order of 0.01 s^{-1}.

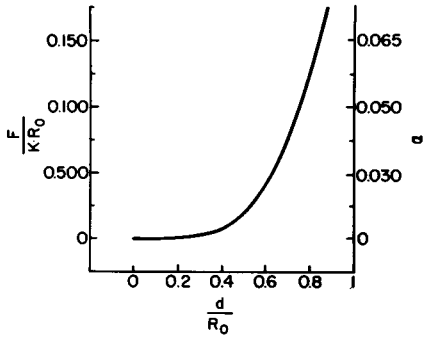

FIGURE 3 A plot of dimensionless force vs. identation calculated assuming that $(\tilde{W} - \tilde{W}_o)_T = (1/2)\ K\alpha^2$. $(\tilde{W})_T$ is the isothermal elastic potential energy density. α is the fractional change in area per molecule. K is the area compressibility modulus. The subscript o refers to the reference state; the superscript ~ means per molecule.

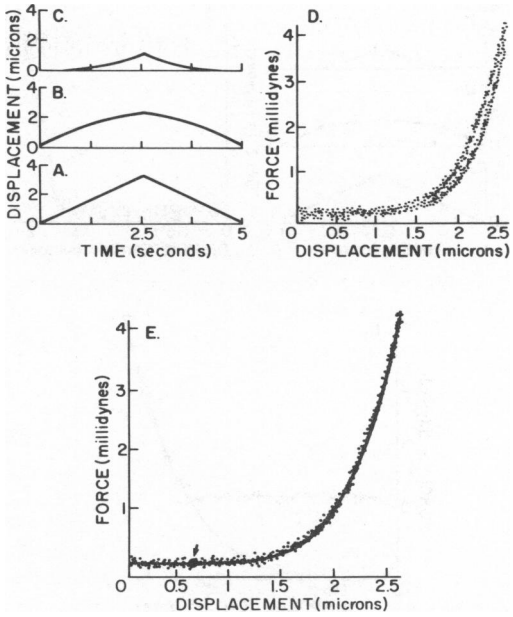

FIGURE 4 Cell poking results for a fully swollen erythrocyte. (*A*, *B*) Change in the vertical poker tip position as a function of time: (*A*) when no contact occurred between poker tip and cell surface; (*B*) when contact occurred. (*C*) Resistive force exerted by the cell surface on the poker tip as a function of time. (*D*) Resistive force as a function of indentation depth. (*E*) Resistive force as a function of indentation depth for the first half period in *D*. The solid curve represents the best fit of the theoretical prediction shown in Fig. 3. This prediction is based on the assumption that shear contributions to changes in the elastic potential energy density are negligible relative to area dilation contributions. The fitted parameters are K, F_o, and X_o. The open circle (with arrow) marks the predicted point of first contact, (X_o, F_o). K, in millidynes per micron, is the elastic area compressibility modulus. Definitions of parameters are more fully explained in the text. In this case, $K = 29.1$ mdyn/μm, $F_o = 0.12$ mdyn, $X_o = 0.62\ \mu$m.

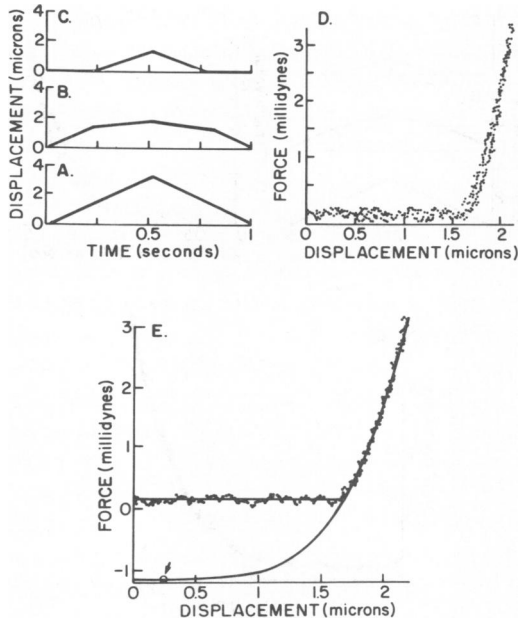

FIGURE 5 Cell poking results for a less than fully swollen cell. Plots are arranged as in Fig. 4. Note that in *E* an additional parameter, X_i, was required to fit these data. $X_i - X_o$ represents the predilation indentation, i.e., the indentation depth, relative to a fully swollen cell, required to initiate membrane stretching. F_i is the calculated value of the force at this indentation depth. (X_o, F_o), marked by the open circle (with arrow), represents a prediction of the point of first contact for the analogous fully swollen cell. $F_i - F_o$ is the value of the force that would have been required to indent a fully swollen cell by the amount $X_i - X_o$. In this case, K = 36.2 mdyn/μm, $F_i - F_o$ = 1.4 mdyn, $X_i - X_o$ = 1.5 μm.

Although the theory developed above has only one undetermined parameter, the elastic area compressibility modulus, we must include other parameters in the fit to account for experimental uncertainties in the geometry of the deformation. Since we do not now have an independent, accurate method for determining the coordinates of the cell surface, we use curve fitting to determine the point of first contact, X_o, between the poker tip and the cell. In some cases we must also fit the indentation depth, X_i, required to initiate membrane stretching. In these cases, this initial indentation occurs with negligible force because even under osmotic conditions where ~80% of the erythrocytes lyse some cells in the population appear to possess initial excess surface area (over that of a sphere of equal volume). Once stretching has begun, however, the geometry of the membrane surface must attain constant mean curvature at equilibrium to achieve minimum potential energy (assuming shear forces are negligible). The total force acting on the poker tip is a function of this initial state of constant mean curvature as well as the instantaneous stretched state. The initial state varies with the surface-to-volume ratio of the unstretched cell. Hence we also vary the initial force, F_o. In contrast to the total force, the incremental force is practically independent of this initial state as discussed below. Thus, given the freedom to translate the axes, every point along the force vs. indentation curve (Fig. 3), calculated based on a one parameter family of surfaces of constant mean curvature, corresponds to some initial stretched state. Our interpretations of these parameters are supported by available experimental evidence also discussed below.

TABLE I
DEPENDENCE OF THE RELATIVE ELASTIC AREA COMPRESSIBILITY MODULUS ON THE RATE OF INDENTATION

Indendation* period	$K/K_{2.5}$‡§	Number of samples
s		
0.5	1.20 ± 0.72	38
2.5	1.00 ± 1.03	73
5.0	1.34 ± 1.00	20

*The indentation period is defined as the half period of the triangle waveform.

‡Values of the elastic area compressibility moduli, K, and their standard deviations for all rates of deformation are normalized by the K value at 2.5 s, $K_{2.5}$.

§The osmolality was ~135 mOsm.

The fitted parameters are K, F_o, X_o, and X_i. Their values are determined by fitting our theoretical curve (Fig. 3) to force vs. indentation data using Curfit, a nonlinear least-squares algorithm (16). K, in millidynes per micron, is the fitted value of the elastic area compressibility modulus. F_o, in millidynes, represents a translation of the ordinate. X_o, in microns, represents a translation of the abscissa. The ordered pair (X_o, F_o) provides a theoretical prediction of the point on the force vs. indentation diagram where initial contact between the poker tip and cell would have occurred if the cell had been fully osmotically swollen. Typically, the fitted value of X_o agrees reasonably with estimates made as follows: the maximum height of the erythrocyte from the glass, measured by the height from the glass at which lateral motions of the tip can first be seen to move the cell, is subtracted from the initial position of the tip, measured by the distance of the tip from the glass coverslip. X_i-X_o, in microns, represents a prediction of the predilation indentation depth, i.e., the indentation depth, relative to a neutrally inflated spherical cell of 6.8 μm, required to achieve membrane stretching and thus to produce the first detectable force increase in our measurement. Appendix B presents a detailed analysis of the logic and assumptions underlying the use of these parameters in constructing a fitting algorithm.

As expected, experiments qualitatively indicate that the predilation indentation depth increases as the osmolality of the swelling medium is increased (Table II). In principle, it is possible to formulate a quantitative test of the predicted value of X_i-X_o as a function of osmotic pressure. Assuming constant surface area, one can calculate the predilation indentation depth as a function of cell volume (Fig. 6). The data of Evans and Fung (14) provide a relation between cell volume and osmotic pressure. Thus, X_i-X_o can be

TABLE II
DEPENDENCE OF FITTED PARAMETERS ON OSMOLALITY

Osmolality‡	K*§	F_i-F_o*	X_i-X_o*	Number of samples
mOsm	*mdyn/μm*	*mdyn*	*μm*	
130	17.9 ± 8.2	0.094 ± 0.167	0.70 ± 0.46	36
140	23.0 ± 17.8	0.31 ± 0.26	1.1 ± 0.4	14
155	34.8 ± 12.0‖	1.6 ± 0.7	1.6 ± 0.2	13
170	26.0 ± 12.8‖	1.9 ± 1.3	1.7 ± 0.5	17

*Mean ± SD. Definitions of the fitted parameters K, F_o, X_o, and X_i are given in the text. The definitions of F_i and F_i-F_o are given in the legend to Fig. 5.

‡The vapor pressure osmometer was calibrated to ±4 mOsm at 100 mOsm.

§The indentation period for all measurements was 2.5 s.

‖Due to increasing X_i-X_o the extraction of K from experimental data becomes less certain as explained in the text.

related to osmotic pressure. In practice, however, this quantitative test is not useful for several reasons. First, the predilation indentation depth is a sensitive function of the assumed surface area of the unstressed cell since this ultimately sets the scale of Fig. 6 (Appendix B). The standard deviation of the surface area for a population of red cells is ~10% of the mean (14). This alone leads to significant uncertainties in X_i-X_o. Second, at osmolalities between 130 and 150 mOsm the average volume within an erythrocyte is a sensitive function of osmolality (14). Small uncertainties in the measured osmolality lead to large uncertainties in average cell volume. Furthermore, the indentation depth is an exceedingly sensitive function of the average volume per cell in this osmolality range (Fig. 6). Third, errors in (X_o, F_o) increase as cell volume decreases because full cell inflation was assumed in scaling the force vs. indentation functions. Fourth, a unique fit, independent of initial guesses for the fitted parameters, can be achieved only when the cells are almost fully swollen, i.e., at osmolalities between 130 and 140 mOsm. This is due to the form of the force vs. indentation curve. Compensatory relations between fitted parameters exist when the initial stretched state is substantially different from a sphere. Finally, random and systematic measurement errors limit the precision and accuracy with which X_i-X_o can be determined. These considerations demonstrate that, although our prediction of the osmotic dependence of the predilation indentation depth agrees qualitatively with experiment, a quantitative test is not possible given experimental uncertainties.

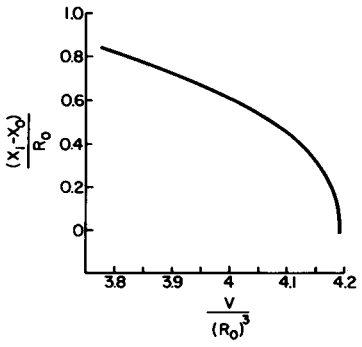

FIGURE 6 A plot of the indentation depth in dimensionless units required to initiate membrane area dilation as a function of cell volume. Shear forces were assumed negligible. As explained in the text regarding Fig. 3, only the portion of this curve corresonding to compression of a cell between two flat plates is strictly accurate (dimensionless indentations <0.325). Small deviations occur as the predilation indentation depth increases further.

Measurements on swollen human erythrocytes gave a range of values for the elastic area compressibility modulus, depending in part on the osmotic conditions, of 17.9 ± 8.2 to 34.8 ± 12.0 mdyn/μm at 25°C. Fractional area expansion >2.6 ± 0.8% produced rapid cell lysis. Table II lists the values of all fitted parameters resulting from poking experiments conducted at various osmolalities. Fig. 7 *A* is a histogram of the elastic area compressibility modulus for a population of 36 erythrocytes swollen in 130 mOsm D-PBS. Fig. 7 *B* is the corresponding probability plot of the distribution function. This modulus had a

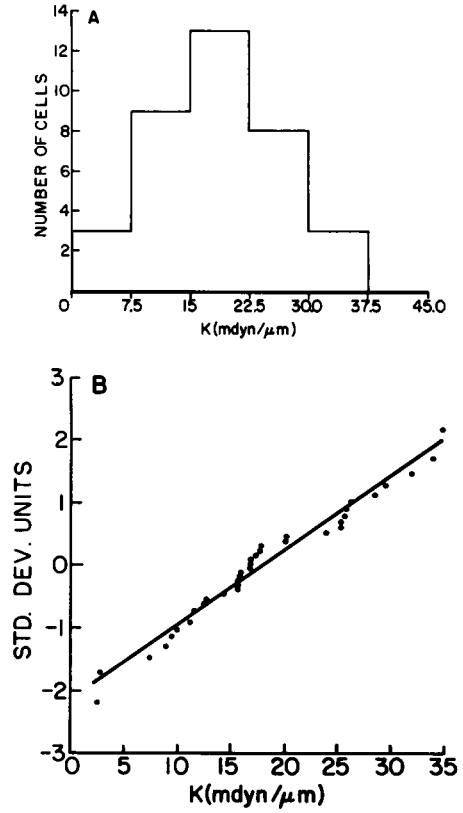

FIGURE 7 (*A*) Histogram of the elastic area compressibility modulus for a population of 36 cells at 25°C and 130 mOsm. The mean and standard deviation are 17 ± 8.2 mdyn/μm. The slightly smaller mean K value at this low osmolality may result from increased osmotic damage to cells. (*B*) A probability plot of the distribution function for the histogram in *A*. The ordinate scale is in standard deviation units from the mean. The distribution of elastic area compressibility modulus is Guassian as is the case for all other osmolalities tested.

Gaussian distribution under all osmotic conditions tested. The true value of the elastic area compressibility modulus is likely to be somewhat larger since these data are corrected for neither the reversible movement of water across the cell membrane in response to hydrostatic pressure gradients nor the presence of osmotically damaged cells. The slightly smaller mean K value at 130 mOsm may result from increased osmotic damage to the cells.

To determine the uncertainty introduced into the K-value distribution function due solely to uncertainty in the fit, we examined the K-value distribution function for theoretical data with imposed noise. Sixty theoretical data curves of 510 points each were generated for fixed values of K, F_o, X_o, and X_i. Uncorrelated Gaussian noise with a defined standard deviation was added to each curve. The magnitude of the standard deviation of the imposed noise was chosen to match the average standard deviation of real data, assuming uncertainty only in the force measurement. These theoretical data curves were then fitted according to the standard fitting routine, and the values of the fitted parameters were examined. Table III lists the means, standard deviations, and ranges of the distributions of the fitted parameters. All fitted parameters were normally distributed when a unique fit was achieved. A unique fit occurs when values of all fitted parameters are independent of initial guesses. Two important conclusions concerning the fitting procedure emerge from these data. First, the fitting procedure accurately determines the values of all fitted parameters in cases where a unique fit is attained. The uncertainty in these values is small compared with the uncertainty of the distribution of real data. This suggests that the standard deviation of the K-value distribution function for highly swollen erythrocytes reflects biological variability or low frequency random experimental errors or both. Second, the capacity of the fitting procedure to determine a unique fit depends on the magnitude of X_i-X_o. If this magnitude is small, the force vs. indentation curve fits smoothly and a unique fit results. Larger values of X_i-X_o yield abruptly rising curves. Due to compensatory relations between fitted parameters for curves of this form, the values of the fitted parameters are sensitive to the initial guesses used. In this regime, accuracy in the determination of the values of the fitted parameters is limited.

TABLE III
THEORETICAL DATA STATISTICS

	K*	F_i-F_o*	X_i-X_o*
	mdyn/μm	*mdyn*	*μm*
Theoretical value	30.0	0.0676	0.700
Fitted value			
mean ± SD	30.0 ± 2.5	0.0514 ± 0.0198	0.695 ± 0.010
distribution range§	24.7–35.5	0.0909–0.0127	0.874–0.445
Theoretical value	30.0	3.96	2.00
Fitted value			
Mean ± SD	‡	‡	‡
Distribution range§	9.35–114	7.40–1.88	3.18–1.17

*Definitions for all parameters are explained in the text or in the legend to Fig. 5. Number of samples equals 60 in all cases.
‡A unique fit, independent of reasonable initial guesses for the fitted parameters, was not achieved.
§The distribution range was determined by varying initial guesses for the fitted parameters over wide ranges, approximately an order of magnitude above and below the theoretical values. Obviously unreasonable fits were excluded.

Using theoretical data, we also simulated the effect of errors in the calibration of the cell poker on the values of fitted parameters. We found that on average a ±15% error in the calibration of displacements propagates into an error of ∓30% in the fitted value of the elastic area compressibility modulus. Errors in the calibration of the bending constant of the horizontal fiber lead to errors of similar magnitude in the value of K.

DISCUSSION

We have used a new method called cell poking to measure the isothermal elastic area compressibility modulus of the erythrocyte membrane. We find good agreement between the measured force vs. indentation data obtained and a theoretical prediction based on a simple membrane model in which surface area is minimized at constant interior volume.

The isothermal elastic potential energy density function, $(\tilde{W} - \tilde{W}_o)_T = (1/2)K\alpha^2$, predicted the observed behavior. The success of this prediction confirmed our assumptions based on the work of Evans and Skalak (8). We assumed that contributions to principal membrane force resultants from shear, bending, and constant surface tensions are negligible in the presence of the large isotropic tensions produced by area expansion. We obtained a range of values for the elastic area compressibility modulus, depending in part on the osmotic conditions, of 17.9 ± 8.2 to 34.8 ± 12.0 mdyn/μm. For highly swollen cells we demonstrated that uncertainty in the mean value of the area modulus due to high frequency noise in the data is small compared with the measured standard deviation. Fractional area expansion >2.6 ± 0.8% produced rapid cell lysis.

Uncorrected for the presence of osmotically damaged cells, these results agree reasonably with those obtained by Evans et al. (4) under similar conditions using micropipette aspiration. They reported a value of 28.8 ± 5.0 mdyn/μm for the elastic area compressibility modulus at 25°C; fractional area expansion >3 ± 0.7% produced immediate cell lysis in their experiment. Subsequently, Evans and Waugh (5) showed that the reversible movement of water across the cell membrane in response to hydrostatic pressure gradients leads to small volume changes (~1% of the total cell volume) during the course of deformation. Correcting for these changes increases the value of the apparent elastic area compressibility modulus measured using micropipette aspiration by approximately one-third (5). The extent of water transport across the cell surface

depends on the geometry (5) and perhaps on the rate of deformation. In the experiments of Evans et al. (4, 5) the rates of deformation are roughly 10-fold faster than in our measurements. We are uncertain how these differences affect the contribution of water transport to the measured elasticity modulus.

The mechanical behavior of swollen erythrocytes provides information restricting possible structural models of the red cell membrane lamina. The major molecular components of this lamina have been isolated and some of their interactions revealed (17, 18). Along with electron microscopy, these biochemical studies have produced a picture of the basic molecular organization of the erythrocyte membrane. Underlying and anchored to the fluid lipid-protein bilayer is a meshwork of cytoskeletal proteins. This meshwork consists of a network of spectrin tetramers and higher oligomers interconnected by short actin filaments and band 4.1. While only this skeletal framework appears to sustain shear (4, 18), both the lipid-protein bilayer and the skeletal framework appear to resist area dilation. For large lecithin bilayer vesicles, Kwok and Evans (19) have shown that the volume-corrected isothermal elastic area compressibility modulus is 14.0 ± 1.6 mdyn/μm. This value is close to the area modulus obtained on erythrocytes in which the spectrin network was partially disrupted by heating the cells to above 50°C (4). These data suggest that the lipid-protein bilayer of the erythrocyte contributes approximately one-third of the total resistive force to area dilation and that the spectrin network contributes the remaining two-thirds. Similar to the lipid-protein bilayer, the spectrin network apparently behaves like a two-dimensional fluid in the presence of large isotropic tensions. The fact that the spectrin skeleton sustains these tensions as a result of only small changes in total red cell surface area suggests that this skeleton does not have much readily accessible excess surface area (over that of the lipid-protein bilayer). This is somewhat surprising since electron micrographs of rotary-shadowed spectrin show the dimer as two loosely intertwined, flexible strands, joined at their ends (20). One might have expected that a network composed of these long, floppy molecules that assume no rigidly defined morphology in vitro would undergo area expansion under substantially smaller tensions than those required to expand the lipid-protein bilayer.

In contrast, the fact that the spectrin network readily undergoes large deformations at constant surface area is consistent with initial expectations based on spectrin's in vitro morphology. This fact, reflected in the relatively small shear modulus of the spectrin matrix, is also consistent with the possibility that the patterns and properties of the links between cytoskeletal elements primarily determine the shear behavior of this matrix. For example, Koppel et al. (21) have proposed that the spectrin network structure is labile, with cross-links continually breaking down and reforming. The capacity of this network to resist stretching suggests restrictions on possible rearrangements. The network must maintain continuity. In addition, it must not undergo rearrangements between laminae of the matrix since this would permit thinning of the matrix resulting in area dilation without large increases in membrane force resultants.

The success of micropipette aspiration experiments on red blood cells encouraged the development of the cell poker, intended primarily for making quantitative mechanical measurements on adherent nucleated cells. Our eventual goal is to understand the contribution of the exoskeleton, plasmalemma, cytoskeleton, and cytoplasmic organelles to the composite mechanical properties of cells. The relatively simple, well-studied swollen erythrocyte provides a model system for establishing the mechanical basis of our measurements and allows us to compare our results with those of micropipette aspiration. A preliminary comparison suggests the following: First, the results from poking swollen red cells agree reasonably with those from micropipette aspiration. This suggests that the primary structural elements in mature red cells that resist area expansion respond similarly to large pushing and pulling deformations. This might not be true for other cell types if, for example, structural elements deep within the cell contribute to forces resisting indentation or if the plasma membrane separates from the underlying cytoskeletal matrix during aspiration. Second, micropipette aspiration is probably the preferred technique for most measurements of the mechanical properties of the erythrocyte membrane. Small forces over a wide dynamic range are readily applied during aspiration. These forces produce large, visually detectable changes in the geometry of the deformed surface, especially in measurements on nonswollen erythrocytes. Control over applied forces and visualization of cell geometry are easier with micropipette aspiration than with cell poking. This may account for the larger standard deviation in our measurement of the elastic area compressibility modulus. Third, cell poking is probably better suited than micropipette aspiration for making mechanical measurements on adherent, spread cells in culture. Because cell poking utilizes indentation, it avoids possible detachment of the plasmalemma from the underlying cytoskeleton that might result from aspiration into a micropipette. Similarly, adhesion between the cell and the poker tip seems less problematic than adhesion between the cell and the inside of the micropipette (22). In addition, contributions of some of the intracellular organelles to composite mechanical properties of the whole cell may be more readily detected using cell poking. Furthermore, precise measurement of horizontal fiber deflections ($<\pm 0.1$ μm) permits force determinations based on small deformations of the unperturbed cell given sufficiently rigid cell structures. These measurements do not depend on visualization of the cell surface. Finally, the design of the poking chamber and direct digital data acquisition make application of cell poking to adherent,

spread cells in culture relatively simple. Comparison of results from cell poking on nucleated cells with those of micropipette aspiration may yield important clues concerning how structural components integrate cellular mechanical forces.

APPENDIX A

The purpose of this Appendix is to provide a fuller discussion of some assumptions that underlie the simplified analysis of cell poking presented in the Theory section. Here we derive closed-form expressions for the local deformation field in a poked red-cell membrane. In contrast, the simplified analysis requires and produces only the shape of the membrane. We begin by adopting the model of Evans and Skalak (8). According to this model the membrane is a two-dimensional elastic structure characterized by a stress-free reference state and an elastic strain-energy density (per unit area in the reference state)

$$W = 1/2(K\alpha^2) + \mu\beta \tag{A1}$$

where K and μ are, respectively, dilational and shear moduli describing the membrane material properties, and α and β are, respectively, area- and shear strain parameters defined as

$$\alpha = \lambda_1 \lambda_2 - 1 \text{ and } \beta = \frac{\lambda_1^2 + \lambda_2^2}{2\lambda_1 \lambda_2} - 1, \tag{A2}$$

where λ_1 and λ_2 are the principal stretch ratios at a point on the membrane.

In the above equations the deformations should be measured from the stress-free reference state. The two most commonly proposed reference states are the biconcave disk and the neutrally inflated sphere (with the same surface area as the biconcave disk). At present it seems impossible to determine which of these possibilities, if either, is correct (23), although the former seems more probable. If the biconcave shape is accepted as stress-free, then the calculation of deformations from this state requires rather elaborate numerical procedures (24). These procedures have indicated that in the transformation from the biconcave disk to the neutrally inflated sphere (*a*) very small increases in internal pressure are required, (*b*) the area strain parameter, α, remains essentially zero, and (*c*) the shear strain parameter, β, varies from zero to ~0.1 over the membrane surface in the inflated state. For simplicity we have adopted the neutrally inflated sphere as the reference state in the following calculations. This assumption makes it possible to obtain relatively simple closed-form expressions for the complete deformation field of the loaded membrane. If the biconcave disk were the correct stress-free shape, then deformations from the neutrally inflated state would be influenced by the presence of modest initial shear strains in that state. However, we do not expect that this would significantly affect our conclusions with regard to our measurements on swollen erythrocytes that, as this Appendix shows, are dominated by area strain.

With respect to the neutrally inflated sphere of radius R_o, the kinematics of the deformation are illustrated in Fig. 2 *B*. The deformation is axially symmetric about the z-axis. A material point on the undeformed sphere is identified by the angular material coordinate σ. The spatial coordinates of this point become $r(\sigma)$ and $z(\sigma)$ as a result of the deformation. Once $r(\sigma)$ and $z(\sigma)$ are known all the important kinematic parameters can be computed, including the principal curvatures

$$\frac{1}{R_\theta} = \frac{1}{r'}\frac{d}{dz}\left[\frac{1}{[1 + r'^2]^{1/2}}\right] \qquad \frac{1}{R_\phi} = \frac{1}{r[1 + r'^2]^{1/2}}, \tag{A3}$$

the principal stretch ratios

$$\lambda_\theta = \frac{1}{R_o}[\dot{r}^2 + \dot{z}^2]^{1/2} \qquad \lambda_\phi = \frac{r}{R_o \sin\sigma}, \tag{A4}$$

and the strain parameters

$$\alpha = \frac{r[\dot{r}^2 + \dot{z}^2]^{1/2}}{R_o^2 \sin\sigma} - 1$$

$$\beta = \frac{R_o^2 \sin\sigma}{2r[\dot{r}^2 + \dot{z}^2]^{1/2}}\left[\frac{\dot{r}^2 + \dot{z}^2}{R_o^2} + \frac{r^2}{R_o^2 \sin^2\sigma}\right] - 1. \tag{A5}$$

In the above equations $(\dot{}) = d/d\sigma$ and $(\,)' = d/dz = \dot{z}^{-1}\, d/d\sigma$.

To solve for the deformation, $r(\sigma)$ and $z(\sigma)$, we can invoke the Principle of Minimum Potential Energy (25). We regard the membrane as an elastic structure undergoing large deformations, and subject to (*a*) a constant enclosed volume constraint, (*b*) displacement constraints at the glass coverslip and at the poker tip, and (*c*) interior pressure loads. Under the constant volume constraint, the pressure loads do no net work so that the potential energy of the system is just the total elastic strain energy of the membrane. The deformation assumed by the membrane at equilibrium will be that which minimizes (subject to the stated constraints) the system's potential energy. Thus we are led to the variational problem, minimize the functional

$$U[r(\sigma), z(\sigma)] = \int_o^\pi \left[\left(\frac{1}{2}K\alpha^2 + \mu\beta\right)2\pi R_o^2 \sin\sigma + \lambda^* \pi r^2 \dot{z}\right] d\sigma, \tag{A6}$$

where λ^* is a Lagrange multiplier associated with the constant volume constraint

$$\pi \int_o^\pi r^2 \dot{z}\, d\sigma = \frac{4}{3}\pi R_o^3. \tag{A7}$$

In cell poking we expect significant area dilation. Thus we write

$$\frac{1}{2}K\alpha^2 + \mu\beta = \frac{1}{2}K\alpha^2\left[1 + \left(\frac{2\mu\beta}{K\alpha^2}\right)\right]$$

and make the a priori hypothesis (to be verified a posteriori) that the deformation will satisfy the condition

$$\left(\frac{2\mu\beta}{K\alpha^2}\right) \ll 1. \tag{A8}$$

With this assumption the variational problem (Eq. A6) reduces to minimizing

$$U^* = \int_o^\pi (\alpha^2 \sin\sigma + \hat{\lambda} r^2 \dot{z})\, d\sigma, \tag{A9}$$

where some constants have been factored out of the integral and the Lagrange multiplier has been appropriately redefined.

It may not be apparent that the problem (Eq. A9) is an area-minimization problem, but this is a fact as shown by the following calculations. The two Euler equations associated with (Eq. A9) are (in view of Eq. A5)

$$\frac{d}{d\sigma}\left(\sin\sigma \frac{\partial \alpha^2}{\partial \dot{r}}\right) - \left(\sin\sigma \frac{\partial \alpha^2}{\partial r} + 2\hat{\lambda} r \dot{z}\right) = 0$$

$$\frac{d}{d\sigma}\left(\sin\sigma \frac{\partial \alpha^2}{\partial z} + \lambda r^2\right) = 0. \tag{A10}$$

The second of these equations can be integrated immediately to give

$$\pm r' = \frac{\left[\left(\frac{2\alpha}{R_o^2}\right)^2 r^2 - (B - \hat{\lambda} r^2)^2\right]^{1/2}}{B - \hat{\lambda} r^2}. \tag{A11}$$

where B is a constant of integration, and Eq. A5 and $r' = \dot{r}/\dot{z}$ have been used in obtaining this equation. Finally using Eq. A5 and Eq. A11 it can be shown that the first of equations in Eq. A10 will be satisfied if and only if α is constant throughout the membrane. Given this last fact, α can be factored out of the integral in Eq. A9, at which point it becomes clear that Eq. A9 is equivalent to the problem of minimizing the surface area of the deformed membrane. To put this another way, if we define the scaled variables as $x = (R_o^2\hat{\lambda}/\alpha)r$, $y = (R_o^2\hat{\lambda}/\alpha)z$, and $2c_s = -(R_o^2\hat{\lambda}/\alpha)^2(B/\hat{\lambda})$, then Eq. A11 becomes

$$\pm\frac{dy}{dx} = \frac{x^2 + 2c_s}{[4x^2 - (x^2 + 2c_s)^2]^{1/2}} \tag{A12}$$

which is precisely the basic equation (Eq. 4) derived in the Theory section as a consequence of the postulated minimum area problem. Further, it is clear that the Lagrange multiplier scaling parameter used in the Theory section is equal to $(R_o\hat{\lambda}/\alpha)$.

For each fixed value of c_s, Eq. A12 can be solved for the deformed shape of the membrane, and once the shape is known the local deformation field can be computed as follows. From the first of equations in Eq. A5 and Eq. A11 it follows that

$$\pm\frac{dx}{d\sigma} = \frac{1}{\nu}\frac{[4x^2 - (x^2 + 2c_s)^2]^{1/2}}{x^2}\sin\sigma, \tag{A13}$$

where the constant $\nu = [2/(1 + \alpha)R_o^2] \cdot (\alpha/R_o^2\hat{\lambda})^2$. This equation holds on those portions of the membrane that are not in contact with flat rigid surfaces (poker tip and coverslip); on the latter portions $(dz/dr) = 0$, so that from the first of equations in Eq. A5 we have

$$\pm\frac{dx}{d\sigma} = \frac{2}{\nu}\frac{\sin\sigma}{x}. \tag{A14}$$

The last equation can be integrated immediately to yield

$$x = \left[\frac{4}{\nu}(1 + \cos\sigma)\right]^{1/2} \quad \text{for} \quad 0 < \sigma < \sigma_t$$

$$x = \left[\frac{4}{\nu}(1 + \cos\sigma)\right]^{1/2} \quad \text{for} \quad \sigma_g < \sigma < \pi, \tag{A15}$$

where σ_t and σ_g are the values of σ at the points of contact between the free membrane and the poker tip and the coverslip, respectively. Eq. A13 integrates to

$$\pm\cos\sigma = A - \nu\gamma E(\psi, k) \text{ for } \sigma_t < \sigma < \sigma_g, \tag{A16}$$

where A is a constant of integration to be determined from continuity conditions, and all the symbols in the last expression on the right-hand side of Eq. A16 have been defined previously in the Theory section entitled General Solution. Eqs. A15 together with $y = y_t$ or $y = y_g$, and Eq. A16 together with Eq. 6 in the Theory section define parametrically the (scaled) deformation $x(\sigma)$, $y(\sigma)$ from the neutrally inflated sphere to the poked configuration.

An examination of this deformation field for the range of loadings encountered in our swollen cell-poking experiments shows that the maximum values of β are of the order of α. Thus,

$$\frac{2\mu\beta}{K\alpha^2} = O\left(\frac{10^{-4}}{\alpha}\right),$$

which is negligible for α as low as 0.001, as was assumed a priori.

APPENDIX B

In principle, fitting the predilation indentation, X_i-X_o, requires a complex recursive algorithm because the force vs. indentation function depends on this parameter in a complex way, i.e., the incremental force is only approximately independent of this parameter. Given the constitutive Eq. 14, the force vs. indentation relation depends only on global area dilation. In turn, area dilation depends on the parameters c_s and λ. For a fixed value of c_s, the scaling parameter λ must be determined to satisfy the volume constraint (Eq. 1) and the boundary conditions (Eq. 13). The boundary conditions (Eqs. 13a and c) are independent of λ. In this range, λ depends only on cell volume. The volume is unknown a priori but can be related to the predilation indentation assuming constant surface area (Fig. 6). Thus, a recursive process could be initiated by providing an initial guess for the volume, then calculating λ, scaling the force vs. indentation function, determining a least-squares fit of X_i-X_o, relating this value to a revised volume estimate, and finally using this estimate to continue the iteration.

In the range in which the radius of the poker tip relative to the radius of the neutrally inflated spherical cell must be specified, i.e., where the λ-dependent boundary condition (Eq. 13b) applies, an even more complicated algorithm would be required. For fixed values of c_s and Rt/R_o in this range, the functional dependence of λ on cell volume (Eq. 7) changes with V_s, which now varies with the degree of inflation. This means that in principle there is a family of force vs. indentation curves. The lower portions of these curves (dimensionless indentations <0.325, Fig. 3) correspond to compression between two flat plates and are mapped onto a universal curve by a scale transformation. The upper portions (dimensionless indentations >0.325, Fig. 3) correspond to indentation by a probe and depend on the functional form of λ. Given that we cannot independently measure the initial volume and surface area of each cell with sufficient accuracy and precision to distinguish which curve of this family should be fit to the data, we rely on arguments presented below that suggest that our fitting algorithm nevertheless allows for an accurate determination of the area compressibility modulus.

In practice, the force vs. indentation function, defined in terms of the four variable parameters described above, depends only weakly on cell volume and the λ-dependent boundary condition. For nearly fully swollen cells, as used in our experiments, the volume is approximately constant over a wide range of predilation indentation depths (Fig. 7). In addition, λ varies slowly with cell volume, i.e., as the reciprocal of the cube root. This means that errors in λ propagate into the force vs. indentation function through the area dilation approximately as errors raised to the two-thirds power. Moreover, the scaled force vs. indentation curve (Fig. 3) is nearly linear over much of the indentation range used in the fit of not fully swollen cells (Fig. 5). Thus, this portion of the curve is relatively insensitive to changes in scale. We expect larger errors in F_o and X_o than in K since the offset (X_o, F_o) depends more strongly on the shape of the initial portion of the curve. Finally, only small errors in λ result from accepting small deviations in the radius of the poker tip relative to the radius of the neutrally inflated spherical cell. These deviations occur only after the radius of contact reaches the radius of the poker tip, and they depend only on the difference between actual cell volume and the volume of an ideal, neutrally inflated spherical cell. Consequently, these deviations lead to only small deviations solely in the upper portion of the force vs. indentation curve relevant to most of our measurements (indentations >1.1 μm).

To support our expectations, we calculated the family of force vs. indentation curves as a function of the initial degree of inflation for an analogous two-dimensional model problem. Over the range of inflation and indentation relevant to our measurements, we found that the upper, higher-load portions of all of these theoretical curves could be made to coincide, approximately, by using the translational freedoms employed in our fitting algorithm. Because these portions primarily determine K we concluded that K could be accurately determined by appropriately fitting the single force vs. indentation curve derived for neutral cell inflation. Therefore, we took the scaling parameter λ to be constant. (This was tacitly assumed in Fig. 3 by writing R_o in place of the true volume-dependent scaling parameter.) Making this assumption greatly simplified the fitting algorithm. We expect the resulting error to be less than the error attributable to experimental uncertainty and biological variability.

The authors thank Professor Carl M. Bender for his lucid and enthusiastic instruction in variational calculus, without which this work would not have been undertaken. We also thank Stephen Felder for valuable programming assistance, Tony Pryse for helpful discussions, and Sharon Fleming for assistance in editing this manuscript.

This work was supported by National Institutes of Health Grants GM27160 and a grant from the Mallinckrodt Foundation. B. Daily is supported by National Institutes of Health Training Grant 5T32GM07200.

Received for publication 7 July 1983 and in final form 26 September 1983.

REFERENCES

1. Petersen, N. O., W. B. McConnaughey, and E. L. Elson. 1982. Dependence of locally measured cellular deformability on position on the cell, temperature and cytochalasin B. *Proc. Natl. Acad. Sci. USA.* 79:5327–5331.
2. McConnaughey, W. B., and N. O. Petersen. 1980. The cell poker: An apparatus for stress-strain measurements on living cells. *Rev. Sci. Instr.* 51:575–580.
3. Ponder, E. 1971. Hemolysis and Related Phenomena. Grune and Stratton, New York.
4. Evans, E. A., R. Waugh, and L. Melnik. 1976. Elastic area compressibility modulus of red cell membrane. *Biophys. J.* 16:585–595.
5. Evans, E. A., and R. Waugh. 1977. Osmotic correction to elastic area compressibility measurements on the red cell membrane. *Biophys. J.* 20:307–313.
6. Hochmuth, R. M., N. Mohandas, and P. L. Blackshear, Jr. 1973. Measurement of the elastic modulus for the red cell membrane using a fluid mechanical technique. *Biophys. J.* 13:747–762.
7. Evans, E. A. 1973. New membrane concept applied to the analysis of fluid shear- and micropipette-deformed red blood cells. *Biophys. J.* 13:941–954.
8. Evans, E. A., and R. Skalak. 1980. Mechanics and Thermodynamics of Biomembranes. CRC Press, Boca Raton, FL.
9. Evans, E. A., R. Kwok, and T. McCown. 1980. Calibration of beam deflection produced by cellular forces in the 10^{-9} – 10^{-6} gram range. *Cell Biophys.* 2:99–112.
10. Aris, R. 1962. Vectors, Tensors and the Basic Equations of Fluid Mechanics, Chapter 10. Prentice-Hall Inc., Englewood Cliffs, NJ.
11. Delaunay, P. C. 1841. Sur la surface de revolution dont la courbure moyenne est constante. *J. de Math.* (Ed.: J. Liouville). 6:309–320.
12. Thompson, D'Arcy W. 1961. On Growth and Form. John Tyler Bonner, editor. Cambridge University Press, London. 49–87.
13. Isenberg, Cyril. 1978. The Science of Soap Films and Soap Bubbles. Tieto Ltd., Clevedon, England.
14. Evans, E. A., and Y. C. Fung. 1972. Improved measurements of the erythrocyte geometry. *Microvasc. Res.* 4:335–347.
15. Johnson, B. S., J. Cronin, and D. Branton. 1978. Coupling polylysine to glass beads for plasma membrane isolation. *Biochem. Biophys. Acta.* 506:81–96.
16. Bevington, P. R. 1969. Data Reduction and Error Analysis for the Physical Sciences. McGraw-Hill, Inc., New York. 204–246.
17. Bennett, Vann. 1982. The molecular basis for membrane-cytoskeleton association in human erythrocytes. *J. Cell. Biochem.* 18:49–65.
18. Branton, D., C. M. Cohen, and J. Tyler. 1981. Interaction of cytoskeletal proteins on the human erythrocyte membrane. *Cell.* 24:24–32.
19. Kwok, R., and E. Evans. 1981. Thermoelasticity of large lecithin bilayer vesicles. *Biophys. J.* 35:637–652.
20. Shotton, D. M., B. E. Burke, and D. Branton. 1979. Molecular structure of human erythrocyte spectrin: Biophysical and electron microscopic studies. *J. Mol. Biol.* 131:303–329.
21. Koppel, D. E., M. P. Sheetz, and M. Schindler. 1981. Matrix control of protein diffusion in biological membranes. *Proc. Natl. Acad. Sci. USA.* 78:3576–3580.
22. Schmid-Schonbein, G. W., K.-L. Paul Sung, H. Tozeren, R. Skalak, and S. Chien. 1981. Passive mechanical properties of human leukocytes. *Biophys. J.* 36:243–256.
23. Fischer, T. M., W. M. Cees, M. Stohr-Liesen, H. Schmid-Schonbein, and R. Skalak. 1981. The stress-free shape of the red blood cell membrane. *Biophys. J.* 34:409–422.
24. Zarda, P. R., S. Chien, and R. Skalak. 1977. Elastic Deformations of Red Blood Cells. *J. Biomechan.* 10:211–221.
25. Fung, Y. C. 1965. Foundations of Solid Mechanics. Prentice-Hall Inc., Englewood Cliffs, NJ. 270–306.